



Fermi National Accelerator Laboratory

FERMILAB-Conf-96/304-E

DØ

**DØ Papers on QCD Studies with Jets
Submitted to DPF '96**

**M. Bhattacharjee, S. Choi, D.E. Cullen-Vidal, M.K. Fatyga,
E. Gallas, S.Y. Jun, J. Krane, J. Perkins, R. Snihur and Y. Yu
For the DØ Collaboration**

*Fermi National Accelerator Laboratory
P.O. Box 500, Batavia, Illinois 60510*

September 1996

*Presented at 1996 Annual Divisional Meeting (DPF 96) of the Division of Particles and Fields of the
American Physical Society, Minneapolis, Minnesota, August 10-15, 1996.*

Disclaimer

This report was prepared as an account of work sponsored by an agency of the United States Government. Neither the United States Government nor any agency thereof, nor any of their employees, makes any warranty, express or implied, or assumes any legal liability or responsibility for the accuracy, completeness or usefulness of any information, apparatus, product or process disclosed, or represents that its use would not infringe privately owned rights. Reference herein to any specific commercial product, process or service by trade name, trademark, manufacturer or otherwise, does not necessarily constitute or imply its endorsement, recommendation or favoring by the United States Government or any agency thereof. The views and opinions of authors expressed herein do not necessarily state or reflect those of the United States Government or any agency thereof.

Distribution

Approved for public release: further dissemination unlimited.

FERMILAB CONF-96/304-E

**DØ PAPERS ON QCD STUDIES WITH JETS SUBMITTED TO
DPF '96**

M. Bhattacharjee, S. Choi, D.E. Cullen-Vidal, M.K. Fatyga, E. Gallas, S.Y. Jun,
J. Krane, J. Perkins, R. Snihur, and Y. Yu
for the DØ Collaboration

Contents

INCLUSIVE JET CROSS SECTION AT DØ	3
M. Bhattacharjee	
THE INCLUSIVE JET CROSS SECTION AT $\sqrt{s} = 630$ GeV AT DØ	6
J. Krane	
THE DIJET MASS SPECTRUM WITH THE DØ DETECTOR	9
S. Choi	
DIJET ANGULAR DISTRIBUTIONS AT DØ	12
M.K. Fatyga	
SUBJET STRUCTURE OF JETS AT DØ	15
R. Snihur	
A STUDY OF MULTI-JET PRODUCTION RATIOS IN $p\bar{p}$ COLLISIONS AT DØ	18
E. Gallas	
SEARCH FOR DOUBLE PARTON SCATTERING IN THE 4 JET CHANNEL AT DØ	21
Y. Yu	
AZIMUTHAL DECORRELATION OF JETS WIDELY SEPARATED IN RAPIDITY AT DØ	24
S.Y. Jun	
COLOR COHERENCE IN $p\bar{p}$ COLLISIONS AT $\sqrt{s} = 1.8$ TeV	27
D.E. Cullen-Vidal	
RAPIDITY GAPS IN HARD PROCESSES AT DØ	33
J. Perkins	

Inclusive Jet Cross Section at DØ

MRINMOY BHATTACHARJEE^a

*Department of Physics & Astrophysics, University of Delhi,
Delhi 110007, India*

Preliminary measurements of the central ($|\eta| \leq 0.5$) inclusive jet cross section for jet cone sizes of 1.0, 0.7 and 0.5 at DØ based on the 1992-93 (13.7pb^{-1}) and 1994-95 (90pb^{-1}) data samples are presented. Comparisons to Next-to-Leading Order (NLO) Quantum Chromodynamics (QCD) calculations are made.

1 Introduction

Leading Order (LO) or $O(\alpha_s^2)$ QCD gives a fair description of the inclusive jet cross section, $\sigma(p\bar{p}) \rightarrow jet + X$, in central pseudorapidities, $|\eta| \leq 1.0$, and over a wide range of center-of-mass(CMS) energies, $0.063 \text{ TeV} < \sqrt{s} < 1.8 \text{ TeV}$ ^{1,2,3}. However, LO comparisons include a 30 – 50% theoretical normalization uncertainty. NLO QCD or $O(\alpha_s^3)$ predictions of the inclusive jet cross section^{4,5,6} reduce theoretical uncertainties to 10 – 20%.

The inclusive jet cross section has been measured at the UA2² and CDF⁷ experiments and more recently, the CDF collaboration has reported an excess in jet production at large E_T relative to NLO QCD expectations⁸. The data recorded by DØ during the 1992-93 and 1994-95 runs are used to measure the inclusive jet cross section for $|\eta| \leq 0.5$. The cone size ($R = \sqrt{(\delta\eta)^2 + (\delta\phi)^2}$) dependence of the inclusive jet cross section, studied at cone sizes of 1.0, 0.7 and 0.5, constitutes a strong test of NLO QCD.

2 Data Sample and Analysis

The DØ detector⁹ has a liquid argon-uranium calorimeter with full pseudo-rapidity ($|\eta| \leq 4.1$) coverage for detection of final state jets. The calorimeter has azimuthal symmetry. The single particle electromagnetic and hadronic resolutions are $15\%/\sqrt{E}$ and $50\%/\sqrt{E}$, respectively.

The detector was read out if a hardware jet trigger based on E_T in calorimeter towers and a subsequent software jet trigger are satisfied. The integrated luminosity for the 1992-93 (1994-95) data sample is 13.7pb^{-1} (90pb^{-1}).

The jets are reconstructed using a cone algorithm with radii of 0.5, 0.7 and 1.0. The E_T of the jet is defined as the sum of E_{Ts} of each tower within the cone. The reconstruction efficiency is 100% in the range of interest.

^aRepresenting the DØ Collaboration.

Fake jets arising from noisy electronic cells, accelerator losses, and cosmic rays are removed by applying offline cuts. The global efficiency of these cuts is $> 95\%$ in $|\eta| \leq 0.5$.

The transverse energy of each jet is corrected for offsets due to underlying events, pileup and uranium noise; showering losses from particles emitted within(outside) the jet cone that deposit some energy outside(inside) the cone; and detector hadronic response¹⁰. At 100 GeV, the mean correction to jet E_T is 17% for 0.7 cone jets. The uncertainty in the correction is $\sim 3\%$ at 100 GeV, which translates into an uncertainty of $\sim 20\%$ in the cross section at 100 GeV for 0.7 cone jets. After energy scale corrections, the cross sections are corrected for jet E_T resolution effects. This correction is of the order of 8% at 100 GeV in $|\eta| \leq 0.5$ for 0.7 cone jets.

3 Results and Conclusions

Figure 1 shows the (Data-Theory)/Theory plot in $|\eta| \leq 0.5$ for 0.7 cone jets. The plot shows cross sections from both the 1992-93 and 1994-95 data, compared separately to a NLO QCD prediction given by JETRAD⁵. The theory is evaluated using the CTEQ2ML parton distribution function (pdf) at a renormalization scale (μ) of $E_T/2$ of the leading jet in the event. The data are in excellent agreement with NLO QCD predictions.

Figure 2 shows the ratio of cross sections (1.0/0.7 and 0.5/0.7) in $|\eta| \leq 0.5$ and $80 \text{ GeV} \leq E_T \leq 480 \text{ GeV}$. This plot shows that the inclusive jet cross section decreases with decreasing cone size. The curves are NLO QCD predictions from JETRAD evaluated using CTEQ2ML at a μ scale of $E_T/2$ of the leading jet in the event. The ratio of cross sections do not depend on the choice of pdfs and parton clustering. However, there is a dependence on the μ scale. Our data seem to prefer a μ scale of $E_T/2$ of the leading jet. Most of the experimental errors (luminosity, selection, unsmearing and a part of the energy scale errors) vanish in a ratio so the systematic errors are expected to be small. These errors are under investigation. The plots show only statistical errors.

In conclusion, our data are in excellent agreement with NLO QCD predictions for production of jets with cone size of 0.7. The ratio of cross sections are in qualitative agreement with NLO QCD predictions and they are independent of pdf and clustering. However, the data seems to prefer $\mu = E_T/2$.

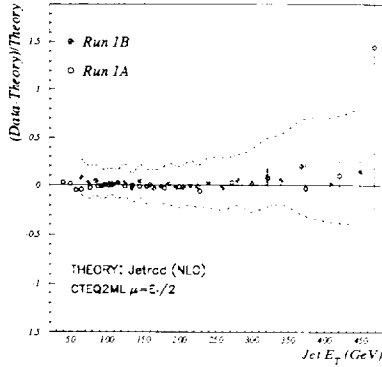


Figure 1: A comparison of the central, $|\eta| \leq 0.5$, inclusive cross section to a NLO QCD calculation with CTEQ2ML evaluated at $\mu = E_T/2$ of the leading jet. The points only include statistical errors. The band represents the total systematic error except the luminosity uncertainty. The solid (open) symbols are for the 1994–1995 (1992–1993) data.

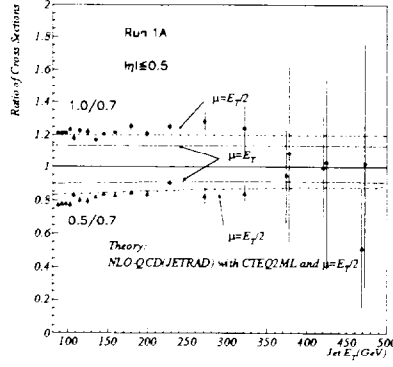


Figure 2: Cross sections for different cone sizes divided by the cross section for 0.7 jets compared to NLO QCD calculations in $|\eta| \leq 0.5$. The solid symbols are from the 1992-93 data. The theory (dotted and dashed dotted lines) is evaluated with CTEQ2ML at $\mu = E_T$ and $E_T/2$ of the leading jet. The errors are statistical. The line at 1 is for reference.

Acknowledgements

We acknowledge the support of the US Department of Energy and the collaborating institutions and their funding agencies in this work.

References

1. T.Akesson *et al.*, (AFS Collaboration), *Phys. Lett. B* **123**, 133 (1983).
2. J.Alitti *et al.*, (UA2 Collaboration), *Phys. Lett. B* **257**, 232 (1991).
3. F.Abe *et al.*, (CDF Collaboration), *Phys. Rev. Lett.* **61**, 613 (1988).
4. S.D.Ellis *et al.*, *Phys. Rev. D* **64**, (1990).
5. W.Giele *et al.*, *Phys. Rev. Lett.* **73**, (1994).-JETRAD
6. Aversa *et al.*, *Phys. Rev. Lett.* **65**, (1990).
7. F.Abe *et al.*, (CDF Collaboration), *Phys. Rev. Lett.* **70**, 1376 (1993).
8. F.Abe *et al.*, (CDF Collaboration), FERMILAB-Pub-96/020-E CDF, Submitted to *Phys. Rev. Lett.* **70**, 1376 (1996).
9. S.Abachi *et al.*, (DØ Collaboration), *Nucl. Instrum. Methods A* **338**, 185 (1994).
10. Jonathan Kotcher for the DØ Collaboration, Proceedings of the 1994 Beijing Calorimetry Symposium, IHEP - Chinese Academy of Sciences, Beijing, China (October, 1994) p. 144.

THE INCLUSIVE JET CROSS SECTION AT $\sqrt{s} = 630$ GeV AT DØ

John Kranc
University of Nebraska
(for the DØ Collaboration)

We present a preliminary measurement of the cross section for central ($|\eta| \leq 0.5$) inclusive jet production at $\sqrt{s} = 630$ GeV using $\sim 400nb^{-1}$ of data collected during the December 1995 Fermilab collider run at DØ. These results are compared to NLO QCD predictions.

1 Introduction

The inclusive jet cross section $\sigma(\bar{p}p) \rightarrow Jet + x$ as a function of jet transverse energy has been measured at $\sqrt{s} = 630$ GeV¹ and comparisons were made to leading order QCD predictions. Next-to-leading order (NLO) predictions which are available now reduce the theoretical uncertainties to less than 20% over the available transverse energy range and have been found to be in good agreement with the inclusive jet cross section measured by DØ at $\sqrt{s} = 1800$ GeV^{2,3}. Comparison of NLO QCD predictions with jet production at a lower center-of-mass energy can lead to a better understanding of QCD.

2 Jet Detection and Reconstruction

Data were recorded with the DØ detector⁴, using triggers requiring localized energy depositions in the calorimeter. Several triggers were used to select jets in various transverse energy ranges.

Jets were reconstructed using a cone algorithm with a cone radius of 0.7 in $\eta - \phi$ space⁵. To remove contamination from electromagnetic objects, cosmic rays, and detector effects, a series of quality cuts were imposed. These included shower shape cuts and a cut on the ratio of the missing transverse energy to the E_T of the leading jet in each event. These cuts were found to be more than 92% efficient in the central region and rejected 95% of all backgrounds.

The transverse energy of each jet was corrected for effects due to the underlying event, detector noise, hadronic energy response, and out-of-cone showering. The corrections applied were typically 20% in the region of interest. The jet transverse energy spectrum obtained after the energy scale correction was then corrected for the distortion due to the finite jet energy resolution (“unsmearing”). The method is described in ref. 5.

3 Results

The $\sqrt{s} = 630$ GeV inclusive jet cross section was compared to several NLO predictions. The theoretical predictions were generated with JETRAD³. The predictions were compared with each other to determine the variation due to different choices of renormalization scales and parton distribution functions. These variations were found to be less than 20% in general.

In Figure 1 we present the resolution-corrected data, the ansatz (“physics curve” used in unsmearing the data), and the CTEQ2ML parton distribution function and renormalization $\mu = E_T/2$ of the leading jet. Also shown is the fractional difference between data and the NLO QCD prediction. There is an additional 13% normalization uncertainty due to luminosity that is not included in the error band. The primary sources of uncertainty in the band are due to the energy scale correction and the unsmearing procedure. The unsmearing correction contribution becomes significant below 55 GeV. The nominal points of the preliminary inclusive jet cross section vs. E_t show shape agreement at a 10% level with NLO QCD predictions for $\sqrt{s}=630$ GeV. The points fell between 20 to 40% lower than the prediction.

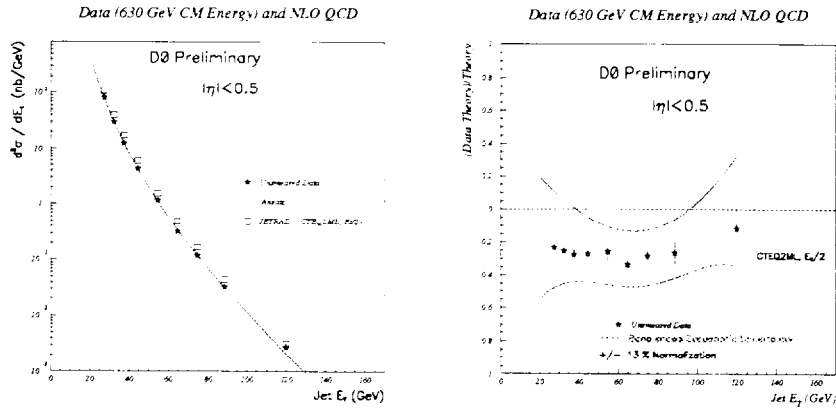


Figure 1: (Left) Inclusive jet cross section shown with JETRAD prediction using CTEQ2ML parton distribution function and renormalization scale of one-half the E_t of the leading jet. (Right) Fractional difference of data and the NLO QCD prediction. Most systematic uncertainties are shown in the band, but an additional 13% normalization uncertainty due to luminosity is not shown.

4 Conclusion

We have presented a preliminary inclusive jet cross section at $\sqrt{s} = 630$ GeV and made a comparison to NLO QCD predictions. Once systematic studies have been completed for the $\sqrt{s} = 630$ GeV analysis, the data set will be compared to that collected at $\sqrt{s} = 1800$ GeV. In the ratio we expect a significant reduction in systematic errors and a precise measurement of jet X_t scaling.

Acknowledgments

We thank the staffs at Fermilab and the collaborating institutions for their contributions to the success of this work, and acknowledge support from the Department of Energy and National Science Foundation (U.S.A.), Commissariat à l'Énergie Atomique (France), Ministries for Atomic Energy and Science and Technology Policy (Russia), CNPq (Brazil), Departments of Atomic Energy and Science and Education (India), Colciencias (Colombia), CONA-CyT (Mexico), Ministry of Education and KOSEF (Korea), CONICET and UBACyT (Argentina), and the A.P. Sloan Foundation.

References

1. UA2 Collaboration, J. Alitti *et al.*, *Phys. Lett. B* **257**, 232 (1991)
2. DØ Collaboration, S. Abachi *et al.*, "Inclusive Jet Cross Section in $\bar{p}p$ collisions with the DØ Detector" submitted to the 28th ICHEP, Warsaw, Poland, July 1996.
3. M. Bhattacharjee, "Inclusive Jet Cross Section at DØ " submitted to DPF96, Minneapolis, Minnesota, August 1996.
4. DØ Collaboration, S. Abachi *et al.*, *Nucl. Instrum. Methods* **A3381851994**.
5. DØ collaboration, S. Abachi *et al.*, *Phys. Lett. B* **357**, 500 (1995).
6. W.T. Giele, E.W.N. Glover, D.A. Kosower, *Phys. Rev. Lett.* **73**, 2019 (1994); *Nucl. Phys.* **B403**, 633 (1993).

The Dijet Mass Spectrum with the DØ Detector

Suyong Choi
for the DØ Collaboration
Seoul National University
151-742 Seoul, Korea

Abstract

We present preliminary results from an analysis of dijet data collected during the 1994-1995 Tevatron Collider run with an integrated luminosity of 91 pb^{-1} . Measurements of dijet mass spectrum distributions in $\bar{p}p$ collisions at $\sqrt{s} = 1.8 \text{ TeV}$ are compared with next-to-leading order QCD theory.

Predictions for the inclusive jet cross section and hence the inclusive dijet cross section have been made using next-to-leading order (NLO) QCD^{3,2,3}. These $\mathcal{O}(\alpha_s^3)$ calculations, which include the possibility of a third radiated parton, reduce theoretical uncertainties to 10–20%. We measure the inclusive dijet mass spectrum in the DØ detector at the Fermilab Tevatron Collider at $\sqrt{s} = 1.8 \text{ TeV}$. Such a measurement, when compared to NLO, constitutes a rigorous test of QCD.

The data sample was collected during the 1994–95 data taking period and corresponds to a luminosity of 91 pb^{-1} . A complete description of the data selection can be found elsewhere⁴. For each event the dijet mass can be calculated (assuming massless jets): $M_{jj}^2 = 2 \cdot E_T^1 \cdot E_T^2 \cdot (\cosh(\Delta\eta) - \cos(\Delta\phi))$, where E_T^1 and E_T^2 are the transverse energies of the two leading E_T jets, $\eta = -\log(\tan \theta/2)$, where θ is the angle from the direction of proton beam at the vertex and ϕ is the azimuthal angle. Cone size of $\mathcal{R}=0.7$ is used. Each event is weighted by the efficiency of the quality cuts applied to the data. The data were collected using four triggers with E_T thresholds of 30, 50, 85 and 115 GeV with integrated luminosities of 0.36, 4.6, 52 and 91 pb^{-1} . These trigger samples were used to measure the dijet mass spectrum above mass thresholds of 200, 270, 370 and 500 GeV where each of the triggers is 100% efficient. The relative normalizations of the four trigger sets is established by requiring equal cross sections in the regions where two trigger sets overlap and are efficient.

The inclusive dijet mass cross sections are computed for two partially overlapping pseudorapidity ranges: $|\eta|_{1,2} < 1.0$, $\Delta\eta < 1.6$ ($|\eta|_{1,2} < 0.5$). The final observed cross section corrected for jet and event selection efficiency is shown in Fig. 1. The combined systematic errors are also shown in Fig 1, ranging from $\sim 13\%$ at 200 GeV to $\sim 55\%$ at 950 GeV. The systematic error is dominated by the uncertainty due to the energy scale with smaller contributions due to

jet selection (1%), vertex selection (1%), the vertex cut (1%), the luminosity scale (8%) and the luminosity matching (0–1.6%).

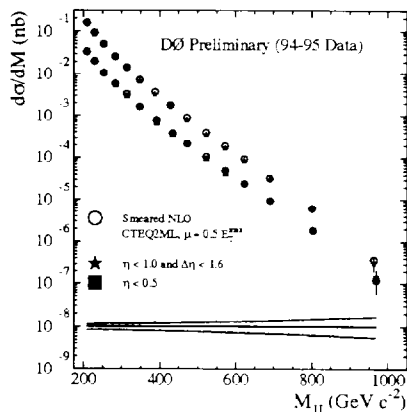


Figure 1: $d\sigma/dM_{jj}$ for $|\eta|_{1,2} < 1.0$, $\Delta\eta < 1.6$ ($|\eta|_{1,2} < 0.5$). The inset solid (dash-dot) curves represent the plus and minus 1σ systematic errors (the dotted lines show the 0, $\pm 25\%$ levels).

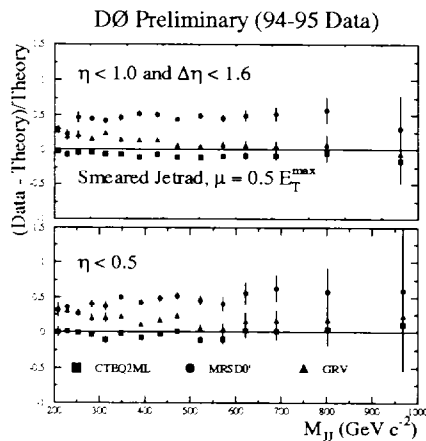


Figure 2: The difference between the data and the smeared NLO QCD predictions normalized to the theoretical prediction $((D - T)/T)$. The symbols represent the calculation using the CTEQ2ML, MRSD0' and GRV pdf's.

Figure 1 also shows a prediction for the inclusive dijet mass spectrum from the NLO parton event generator JETRAD³. The NLO calculation of the dijet mass spectrum has been smeared by the measured jet resolutions. There is good agreement between the prediction and the data over seven orders of magnitude. The data and theoretical calculation are binned identically in M_{jj} bins. The NLO calculation requires specification of the renormalization and factorization scale ($\mu = E_T/2$ where E_T is the maximum jet E_T in the generated event), parton distribution function (pdf) (CTEQ2ML⁶), and a parton clustering algorithm. Partons within $1.3 \mathcal{R}$ of one another were clustered if they were also within $\mathcal{R}=0.7$ of their E_T weighted η, ϕ centroid. The value of $1.3 \mathcal{R}$ was determined by overlaying jets in data from separate events and determining the separation at which the jet reconstruction algorithm could resolve the individual jets. Variation of the pdf can alter the prediction by up to 20% depending on M_{jj} . Variation of μ between $0.25E_T$ to E_T can alter the predictions normalization by 10–20% with some M_{jj} dependence. In addition the choice of parton clustering between $1.3 \mathcal{R}$ and $2.0 \mathcal{R}$ alters the

normalization by $\sim 5\%$ with a small (2-3%) M_{jj} dependence.

Figure 2 shows the ratio, $(D - T)/T$, for the data (D) and the NLO theoretical predictions (T) based on the CTEQ2ML⁶, MRSD0'⁷ and GRV⁸ pdf's. Given the experimental and theoretical uncertainties the predictions are in excellent agreement with the data. The CTEQ2ML pdf gives the best agreement for the absolute normalization.

In conclusion, we have measured the inclusive dijet mass spectrum for $|\eta|_{1,2} < 1.0$, $\Delta\eta < 1.6$ ($|\eta|_{1,2} < 0.5$) and $200 < M_{jj} < 1100$ GeV at $\sqrt{s} = 1.8$ TeV. The QCD NLO model, using different pdf's is in excellent agreement with the M_{jj} dependent shape of the observed inclusive dijet mass spectrum.

Acknowledgments

We thank the staffs at Fermilab and the collaborating institutions for their contributions to the success of this work, and acknowledge support from the Department of Energy and National Science Foundation (U.S.A.), Commissariat à l'Energie Atomique (France), Ministries for Atomic Energy and Science and Technology Policy (Russia), CNPq (Brazil), Departments of Atomic Energy and Science and Education (India), Colciencias (Colombia), CONACyT (Mexico), Ministry of Education and KOSEF (Korea), CONICET and UBACyT (Argentina), and the A.P. Sloan Foundation.

References

1. W.T. Giele, E.W. Glover, and D.A. Kosower, Phys. Rev. Lett. **73**, 2019 (1994) and private communications. We use the program JETRAD written by these authors.
2. S.D. Ellis, Z. Kunszt, and D.E. Soper, Phys. Rev. Lett. **64**, 2121 (1990.)
3. F. Aversa, *et al.*, Phys. Rev. Lett. **65**, (1990)
4. S. Abachi *et al.*, (DØ Collaboration), FERMILAB-CONF-96/168-E
5. S.D. Ellis, Z. Kunszt and D.E. Soper, Phys. Rev. Lett. **69**, 3615 (1992)
6. J. Botts *et al.*, (CTEQ Collaboration), Phys. Rev. **D51**, 4763 (1994)
J. Botts *et al.*, (CTEQ Collaboration), Phys. Lett. **B304**, 159 (1993)
7. A.D. Martin, R.G. Roberts, and W.J. Stirling, Phys. Lett. **B306**, 145 (1993) and erratum Phys. Lett. **B309**, 492 (1993)
8. M. Glück, E. Reya and A. Vogt, Zeit. Phys. **C53**, 127 (1992)

DIJET ANGULAR DISTRIBUTIONS AT DØ

M. K. FATYGA
(for the DØ Collaboration)
*University of Rochester, Rochester,
NY 14627, USA*

Measurements of the dijet angular distributions are relatively insensitive to parton distribution functions and thus offer an excellent method of testing the LO and NLO predictions of perturbative QCD. We present measurements of the dijet angular distributions for $|\eta| < 3.0$ in $p\bar{p}$ collisions at $\sqrt{s} = 1.8$ TeV.

1 Introduction

The dijet angular distribution allows us to measure the properties of parton-parton scattering without strong dependence on the details of the parton distribution functions. At small center of mass scattering angles, the dijet angular distribution predicted by leading order QCD is proportional to the Rutherford cross section: $d\hat{\sigma}_{ij}/d\cos\theta^* \sim 1/\sin^4(\frac{\theta^*}{2})$, where θ^* is the center of mass scattering angle. It is useful to measure the angular distribution in the variable χ , rather than $\cos\theta^*$, where $\chi = (1 + \cos\theta^*)/(1 - \cos\theta^*) = e^{|\eta_1 - \eta_2|}$. The dijet angular distribution is plotted in the variable χ in order to flatten out the distribution and facilitate an easier comparison to the predictions of QCD¹. In addition, the dijet angular distribution provides a test for possible quark compositeness.

The quantity measured in this analysis is $1/N(dN/d\chi)$, in bins of the dijet mass M_{jj} . The other variables of interest are the center-of-mass pseudorapidity of the dijet pair, $\eta^* = \frac{1}{2}(\eta_1 - \eta_2)$, and the pseudorapidity boost: $\eta_{\text{boost}} = \frac{1}{2}(\eta_1 + \eta_2)$.

2 Event Selection

The DØ detector is described elsewhere². An inclusive two-jet sample was used. The two leading E_T jets were required to have a pseudorapidity less than 3.0. Four mass bins were then chosen so that the trigger was fully efficient whilst maximizing the statistics and χ reach (χ_{max}). A cut was then made on the η_{boost} of the dijet system so that there was uniform acceptance for the χ range being examined. The mass, χ , and η_{boost} ranges are described in Table 1.

Min E_{T1}	Mass			χ_{max}	$ \eta_{boost_max} $
55	260	—	425	20	1.5
120	475	—	635	13	1.5
120		> 550		18	1.5
175		> 635		11	1.5

Table 1: The mass bins and their χ and η_{boost} ranges.

3 Results

QCD predictions at leading order (LO) and next to leading order (NLO) were calculated using JETRAD³. In this calculation, the CTEQ3M parton distribution functions were used with a renormalization scale equal to the transverse energy of the leading jet. The theoretical prediction was smeared in E_T and η in order to compare it to data. The data are compared to the LO and NLO predictions of QCD in Fig 1. Fig 2 illustrates the effect on the highest mass bin of adding a contact term for quark compositeness. Since an added contact term is not yet available at NLO, its effect was calculated using LO Papageno⁴. The NLO JETRAD was then multiplied by the ratio of LO with and without the contact term, to produce the curves shown.

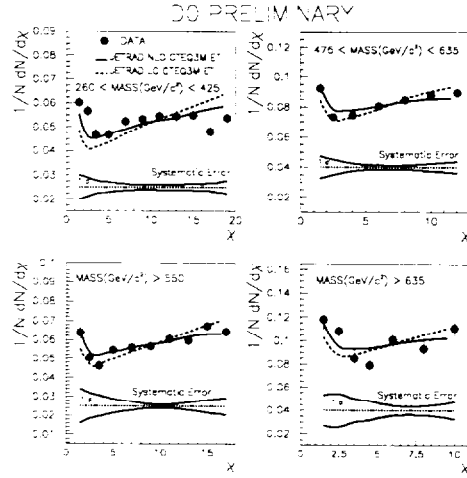


Figure 1: Comparisons of data to NLO and LO predictions of QCD using JETRAD with CTEQ3M and a renormalization scale of E_T . The errors bars are statistical. Shown at the bottom of each plot is the plus and minus 1σ systematic error band.

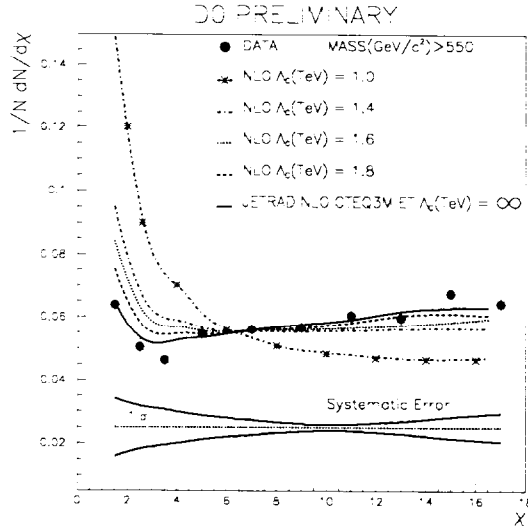


Figure 2: Comparison of data to NLO prediction of QCD using JETRAD with CTEQ3M and a renormalization scale of E_T with an added contact term for quark compositeness. The error bars are statistical. Shown at the bottom of the plot is the plus and minus 1σ systematic error band.

4 Conclusion

The NLO predictions of QCD agree well with the measured dijet angular distributions in all mass bins, including those which would be affected by the addition of a contact term for quark compositeness.

References

1. R. K. Ellis and W. J. Stirling, 'QCD and Collider Physics', FERMILAB-Conf-90/164-T, August 1990, p. 66-69.
2. S. Abachi *et al.*, (DØ Collaboration), *Nucl. Instrum. Methods*, **A338**, 185 (1994).
3. W.T. Giele, E.W. Glover, and D.A. Kosower, *Phys. Rev. Lett.*, **73**, 2019 (1994) and private communications.
4. I. Hinchliffe, 'The Papageno Partonic Monte-Carlo Program', LBL-34372, July 1993.

SUBJET STRUCTURE OF JETS AT DØ

R. SNIHUR
(for the DØ Collaboration)
*Northwestern University, Evanston,
IL 60208, USA*

We present a preliminary study of jet structure in $\bar{p}p$ collisions at $\sqrt{s} = 1.8$ TeV using data taken with the DØ detector during the 1994-95 Tevatron run. We measure the average number $\langle N_{s,ub} \rangle$ and radial distributions of subjets within a jet, and compare to the predictions of HERWIG 5.8, a parton-shower Monte Carlo event generator.¹

1 Introduction

In leading order perturbative QCD, jets are formed from the final state of a hard body 2-to-2 scatter of partons. Jets are pencil-thin at this order, consisting of a single parton carrying the full jet transverse energy E_T in a definite direction in $\eta - \phi$ space. Next-to-leading order calculations predict jets containing two partons. A two parton jet will have its E_T distributed in $\eta - \phi$ space, giving structure to the jet. Similarly, higher order radiation and non-perturbative hadronization further contribute to jet structure. Using a cone jet algorithm, DØ has studied the E_T flow over various subcones within each jet.² For the analysis presented here, we use the k_T jet algorithm, a variation of the Durham jet algorithm modified for hadron-hadron collisions.³ We study jet structure by rerunning the k_T jet algorithm within jets to resolve subjets.⁴ This method is used to directly compare calorimeter cells, hadrons and partons, and is expected to have small hadronization and detector corrections.⁵

In the k_T jet algorithm, all 4-vectors in the event are merged together successively starting with the pair with the smallest relative p_T , stopping when no pair is within a distance $D = 1.0$ in $\eta - \phi$ space. The remaining 4-vectors are called jets. To resolve subjets within a jet, the algorithm is rerun on all 4-vectors within the jet. Merging stops when all 4-vector pairs (i,j) have

$$d_{i,j} = \min(E_{T,i}^2, E_{T,j}^2)(\Delta\eta_{i,j}^2 + \Delta\phi_{i,j}^2) > y_{cut} E_{T,jet}^2$$

The resolution parameter $0 \leq y_{cut} \leq 1$ defines the minimum relative transverse momentum between any two subjets inside the jet. For $y_{cut} = 1$, the number of subjets within any jet always equals one and increases as $y_{cut} \rightarrow 0$.

2 Data Analysis

Inclusive jet events were reconstructed by preclustering calorimeter cells within a radius 0.2 in $\eta - \phi$, then clustering using the k_T jet algorithm. Subjets were resolved within jets with $275 < E_T^{jet} < 350$ and $|\eta_{jet}| < 0.5$ at a series of y_{cut} values. Figure 1 shows that $\langle N_{sub} \rangle$ increases by $\sim 70\%$ as y_{cut} is decreased three orders of magnitude and $\langle N_{sub} \rangle \approx 1.25$ at $y_{cut} = 10^{-2.0}$. HERWIG subjets at the parton level (after parton showering) account for $\geq 70\%$ of the subjets observed in DØ jets. $\langle N_{sub} \rangle$ increases only slightly when the analysis is redone in HERWIG at the particle level, showing that hadronization effects are small for these y_{cut} , although this may be model dependent. When the detector simulation is included, HERWIG agrees with the DØ data quite well, quantifying the effects of showering in the DØ calorimeter.

Choosing $y_{cut} = 10^{-2.0}$ forces the subjets in these high E_T jets to be separated by distances ≥ 0.2 in $\eta - \phi$ space and $E_T^{sub} > 27$ GeV. Figure 2 shows the $\langle N_{sub} \rangle$ resolved within a distance ΔR from the jet axis. On average, there is approximately one subjet resolved within $\Delta R \leq 0.25$, and very few additional subjets for $\Delta R > 0.7$. For jets with two subjets, it is most likely that one subjet carries most of the jet E_T near the jet axis, and the second subjet is much softer and further from the jet axis. This interpretation is confirmed by Figure 3, which is Figure 2 weighted by the subjet E_t fraction.

$$\langle \rho(\Delta R) \rangle = \frac{\sum_{i=1}^{N_{sub}(r \leq \Delta R)} E_{T,i}}{\sum_{i=1}^{N_{sub}(r \leq 1.0)} E_{T,i}}$$

reaches a plateau at smaller ΔR than $\langle N_{sub} \rangle$, with subjets at $\Delta R > 0.25$ contributing $< 10\%$ to the total jet E_T .

In conclusion, HERWIG with the detector simulation agrees well with the DØ data. In HERWIG, particle and parton level jets agree well with each other, but have less (more) subjets than the jets at the calorimeter level, for distances ΔR greater (less) than 0.2, and have relatively more (less) E_T concentrated in the jet core.

References

1. G. Marchesini *et al* *Computer Phys. Commun.* **67**, 465 (1992)
2. DØ Collaboration, S. Abachi *et al*, *Phys. Lett. B* **357**, 500 (1995).
3. K.C. Frame in *Proc. DPF94*, (Albuquerque, 2-6 August, 1994).
4. R.V. Astur in *Proc. 10th $\bar{p}p$ Workshop*, (Batavia, IL, 1995.)
5. M.H. Seymour in *Proc. 10th $\bar{p}p$ Workshop*, (Batavia, IL, 1995.)

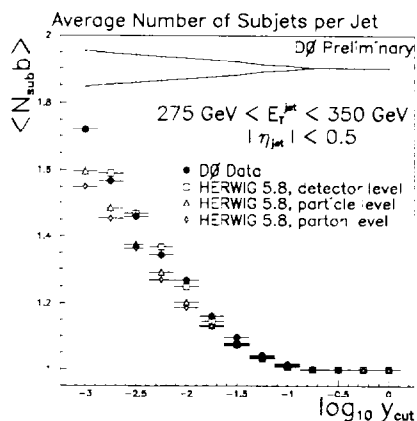


Figure 1: Average number of subjets per central high E_T jet vs. resolution variable y_{cut} . The error bars are statistical, and the $\pm 1\sigma$ systematic error band is an estimate of the effects of multiple interactions and energy scale correction error, added in quadrature.

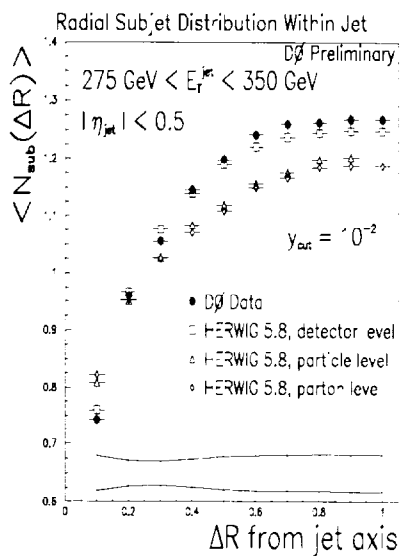


Figure 2: Average number of subjets per jet within a radius ΔR around the jet axis. The error bars are statistical, and the systematic error band is $\pm 1\sigma$.

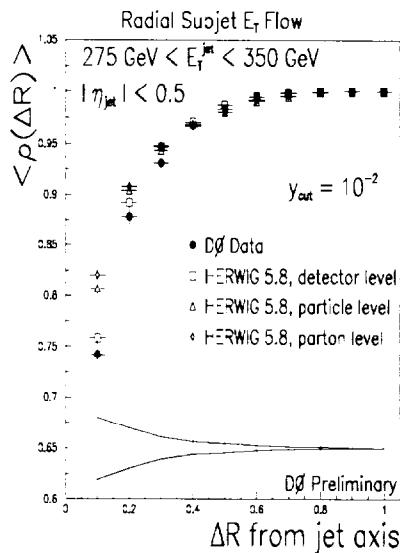


Figure 3: The average E_T fraction carried by subjets within a radius of ΔR around the jet axis. The error bars are statistical, and the systematic error band is $\pm 1\sigma$.

A STUDY OF MULTI-JET PRODUCTION RATIOS IN $p\bar{p}$ COLLISIONS AT DØ

ELIZABETH GALLAS
(for the DØ collaboration)
University of Texas at Arlington,
Arlington, Texas 76019, USA

We study inclusive jet multiplicity ratios in multi-jet events from $p\bar{p}$ collisions at $\sqrt{s} = 1.8$ TeV recorded using the DØ detector at the Fermilab Tevatron collider. Preliminary average multi-jet production ratios are presented as a function of the scalar jet transverse energy and compared to NLO calculations.

1 Introduction

In $p\bar{p}$ collisions at center-of-mass energy $\sqrt{s} = 1.8$ TeV, the primary manifestation of QCD (Quantum Chromodynamics) in the DØ detector is the production of jets. Typically, the interaction of single parton constituents of a proton and an antiproton produce two hard back-to-back jets and some fraction of the time, additional distinct jets are produced. Jet reconstruction algorithms are employed to reconstruct the initial energy and direction of the outgoing partons from the primary interaction and subsequent radiation. The purpose of this analysis is to study the scale of multi-jet emission in events with two or more jets. We compare the event rate for inclusive three jet production to inclusive two jet production and compare to NLO predictions.

2 Analysis and Comparison to NLO

The ~ 10 pb⁻¹ of data used in the current analysis were recorded during the 1992-1993 Tevatron collider run. The essential detector components used were the calorimeter for the identification and measurement of jets and the central tracking chambers to measure the interaction vertex. The DØ detector is fully described elsewhere ¹.

Events were recorded using five inclusive triggers each requiring at least one jet above a transverse energy (E_T) threshold in the calorimeter. These thresholds were 20, 30, 50, 85 and 115 GeV. Jets were reconstructed using a fixed cone algorithm of radius $R = \sqrt{\eta^2 + \phi^2} = 0.7$. Cuts were applied to eliminate fake jets arising from calorimeter noise, cosmic rays, electromagnetic objects, and multiple interactions. In the data analysis and the theoretical calculation, jets contributed to the jet multiplicity if the jet pseudorapidity

$|\eta_{jet}| < 3.5$.

We measure the inclusive 3-jet to 2-jet ratio

$$\frac{\sigma_3}{\sigma_2} = \frac{\sigma(p\bar{p} \rightarrow n \text{ jets} + X; n \geq 3)}{\sigma(p\bar{p} \rightarrow m \text{ jets} + X; m \geq 2)} \quad (1)$$

as a function of $H_T = \sum E_T$, where the sum is over all jets above a minimum E_T threshold.

Figure 1 shows the measured ratio for E_T thresholds of 20 and 30 GeV as a function of H_T . The error bars indicate the statistical uncertainty only. The ratio rises steeply as H_T increases to 300 GeV, then levels off and perhaps decreases slightly at higher H_T .

The data were compared to theoretical predictions of Summers and Zepfenfeld² who used a variation of JETRAD³, a next-to-leading (NLO) order QCD Monte Carlo. These authors assumed MRSD' structure functions and a renormalization scale of $\mu_R = H_T/4$ for the 2 leading jets. Two variations on the renormalization scale for the third jet were used, one with $\mu_R^{(3)} = H_T/4$ and the other having $\mu_R^{(3)} = E_T^{(3)}$, where $E_T^{(3)}$ is the transverse energy of the third jet. In the figure, the dotted and dashed curves indicate the theoretically predicted ratio at the same E_T thresholds for the two different renormalization scale prescriptions for the third jet.

Reasonable agreement between the theory and the data is seen for both E_T thresholds. However, the data corresponding to the 30 GeV E_T threshold clearly prefer the softer renormalization scale for the third jet.

Calculations of systematic uncertainties associated with the measurement are underway. Uncertainties introduced by calorimeter noise or cosmic rays, shown to be constant in H_T , change the central value of the ratio by no more than about 2%. Somewhat larger uncertainties are seen due to the jet energy scale and multiple interactions which are H_T dependent. These vary from 6 to 7% respectively at low H_T and from 3 to 5% at the highest H_T . Also underway are further comparisons of these results to other Monte Carlo predictions.

3 Conclusions

We have measured the ratio σ_3/σ_2 as a function of the total transverse energy H_T . NLO QCD predictions are in reasonable agreement with this measurement. These preliminary results indicate that a softer normalization scale for multijet emission may be preferred over the scale of the hard scattering process.

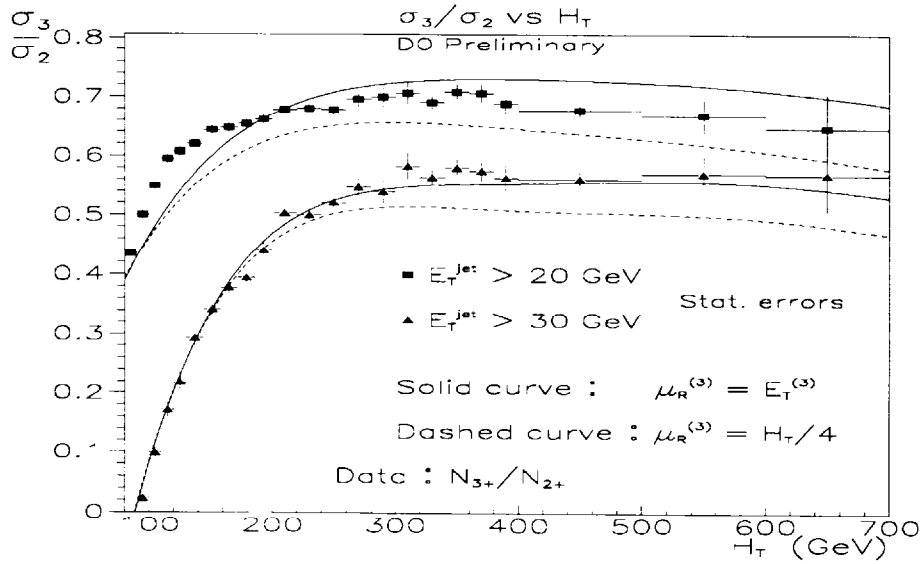


Figure 1: Measured (data points) and predicted values (dotted/dashed curves) of σ_3/σ_2 as a function of H_T , for minimum E_T thresholds of 20 and 30 GeV.

Acknowledgments

We thank David Summers and Dieter Zeppenfeld for many stimulating and helpful discussions. Also, we thank the staffs at Fermilab and the collaborating institutions for their contributions to the success of this work, and acknowledge support from the Department of Energy and National Science Foundation (U.S.A.), Commissariat à L'Energie Atomique (France), Ministries for Atomic Energy and Science and Technology Policy (Russia), CNPq (Brazil), Departments of Atomic Energy and Science and Education (India), Colciencias (Colombia), CONACyT (Mexico), Ministry of Education and KOSEF (Korea), CONICET and UBACyT (Argentina), and the A.P. Sloan Foundation.

1. DØ collaboration, S.Abachi et al., *Nucl. Instrum. Methods A* **338**, 1 (8)5(1994).
2. D. Summers and D. Zeppenfeld, 'Minijet activity in high- E_T jet events at the Tevatron,' September 1995, [hep-ph/9509206](#).
3. W.T. Giele, E.W.N. Glover and D.A.Kosower, *Nucl. Phys. B* **403** (1993) 633.

SEARCH FOR DOUBLE PARTON SCATTERING IN THE 4 JET CHANNEL AT DØ

YEONSIK YU
FOR THE DØ COLLABORATION
Department of Physics, Seoul National University
Seoul 151-742, Korea

We have searched for double parton scattering in the 4-jet channel with an integrated luminosity of 4.4 pb^{-1} , collected using the DØ detector during 1994-1995 Fermilab Collider run at a center of mass energy (\sqrt{s}) of 1.8 TeV. We present the preliminary observation of a statistically significant excess of signal.

1 Introduction

In the Standard Model, most 4 jet events are produced by the QCD process of gluon Double Bremsstrahlung (DB). Recently, there has been increasing interest in the search for another mechanism called Double Parton Scattering (DPS).¹ DPS is important because it is sensitive to parton correlations within the proton.

2 Data Selection

A detailed description of the DØ detector can be found elsewhere.² The initial hardware trigger selected inelastic $\bar{p}p$ collisions as indicated by counts in forward hodoscopes. The next trigger stage required transverse energy (E_T) in at least two calorimeter tiles above a preset threshold of $E_T > 5$ GeV. A tile corresponds to a $\Delta\eta\Delta\phi$ area of 0.2 units in pseudorapidity(η)-azimuth(ϕ) space. The selected data were then processed through a software trigger, which required 4 jets with E_T above 10 GeV reconstructed with DØ $R=\sqrt{(\Delta\eta)^2 + (\Delta\phi)^2}=0.3$ cone algorithm. Additional offline selections were applied to the data, as summarized in Table 1. Jets with cones of $R=0.7$ were used subsequently in the offline analysis.

3 Data Analysis

The search for DPS proceeded by using a neural network to differentiate between DB and DPS processes. The JET_NET V3.4 software⁴ was used for this purpose. After many trials of various combinations of nodes, we chose a configuration for the network consisting of 10 input nodes, 19 hidden nodes

Table 1: Summary of offline data selection

Selection	Number of Events left after cut
Total Number of Events	805,256
≥ 4 Jets	641,476
E_T of Jets > 25 GeV	91,014
Standard Jet Quality Criteria ³	82,234
Single Interaction	18,203

and 1 output node. For the 10 input nodes, the variables were the space angle combinations between the 1st and the 2nd and between the 3rd and 4th jet (ordered in E_T), the ratios of E_T values for the 6 combinations of the leading 4 jets, as well as the following variables:

$$S \equiv \left[\left\{ \left(|\vec{P}_T^i + \vec{P}_T^j| / \sqrt{P_T^i + P_T^j} \right)^2 + \left(|\vec{P}_T^k + \vec{P}_T^l| / \sqrt{P_T^k + P_T^l} \right)^2 \right\} / 2 \right]^{\frac{1}{2}}$$

$$\Delta_S \equiv \cos^{-1} \left[\frac{\{(\vec{P}_T^i + \vec{P}_T^j) \cdot (\vec{P}_T^k + \vec{P}_T^l)\}}{\{|\vec{P}_T^i + \vec{P}_T^j| \cdot |\vec{P}_T^k + \vec{P}_T^l|\}}, \right]$$

where \vec{P}_T^i is the transverse momentum vector for the i^{th} jet. The S and Δ_S that corresponded to combinations of jets with smallest value of S were used as the inputs to the neural network.

To train the neural network, we made separate samples of DB and DPS events. For the DB sample, we chose an independent data set of inclusive 4-jet events that satisfied our data-selection criteria. For the DPS sample, we combined two inclusive jet events that also satisfied our data-selection criteria (again, using an independent data set). Applying the above conditions, the training assigned the output 0 and 1 to the DB and DPS, respectively.

Subsequently, we generated DB Monte Carlo events using Pythia V5.7,⁵ and passed these through the neural network. The Pythia events were generated at the particle level, and smeared to account for energy and position resolution of the detector. We also processed our data through the neural network. The outputs of both the Pythia DB Monte Carlo and the data are shown in Fig. 1. The output for the Pythia events is normalized to the output for the data below the value 0.1. There is a statistically significant excess at large output values, suggesting that the data cannot be described with DB alone. DPS Monte Carlo events generated with Pythia are being studied to extract the fraction of DPS events from the data.

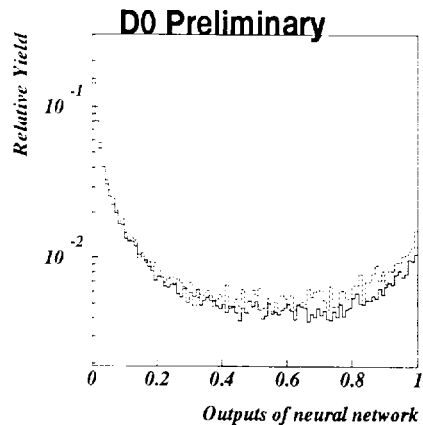


Figure 1: Neural network outputs for DB Pythia Monte Carlo (Solid line) and Data (Dashed).

4 Conclusions

We have performed a search for the DPS process using a neural network procedure and have observed a statistically significant excess in the region expected for DPS. A study is currently underway to extract the DPS fraction.

1. CDF Collaboration, *Phys. Rev. D* **47**, 4857 (1993); UA2 Collaboration, *Phys. Lett. B* **268**, 145 (1991) AFS Collaboration, *Z. Phys. C* **34**, 163 (1987).
2. DØ Collaboration, *Nucl. Instrum. Methods A* **338**, 185 (1994).
3. M. Bhattacharjee et al., DØ internal note 2197.
4. Lonnblad et. al., *Comp. Phys. Comm.* **81**, 185 (1994).
5. T. Sjostrand, *Comp. Phys. Comm.* **82**, 74 (1994); *Phys. Rev. D* **36**, 2019 (1987); Pythia provides all QCD contributions to ≥ 4 -jet events, including the dominant DB process.

AZIMUTHAL DECORRELATION OF JETS WIDELY SEPARATED IN RAPIDITY AT DØ

SOON YUNG JUN
Northwestern University
(for the DØ Collaboration)

We present preliminary results from an analysis of the azimuthal decorrelation of dijet events as a function of their separation in pseudorapidity using the data collected during the 1994-1995 collider run. These results are compared to a parton shower Monte Carlo (HERWIG) and a theoretical prediction using BFKL resummation.

1 Introduction

The exponential growth of the dijet inclusive cross section with increasing rapidity interval between the tagging jets at the extremes of rapidity was originally proposed as a signature of the QCD perturbative pomeron¹. This is the prediction of the color singlet solution of the Balitsky, Fardin, Kuraev, and Lipatov (BFKL) equation² obtained by resumming the leading logarithmic contributions to the radiative corrections to parton scattering in the high-energy limit. At a fixed collider energy, the azimuthal angle decorrelation of jets widely separated in rapidity was suggested as an alternative approach to search for the effect^{3,4}. The broadening of distribution in the azimuthal angle difference with increasing dijet rapidity interval is a characteristic feature of BFKL dynamics. The first measurement of the azimuthal decorrelation between jets with pseudorapidity separation up to five units was previously reported by the DØ collaboration⁵.

We have extended this measurement of the azimuthal decorrelation by employing a lower, symmetric P_T threshold cut (20GeV) and allowing a pseudorapidity separation up to six units with a substantial amount of new data collected by the DØ detector⁶ during the 1994-1995 collider run. We report preliminary results for the $\Delta\phi$ distribution and for $\langle\cos(\pi - \Delta\phi)\rangle$ as a function of $\Delta\eta$, where $\Delta\phi = \phi_1 - \phi_2$ is the difference in azimuth of the two tagging jets and $\Delta\eta = \eta_1 - \eta_2$ is the difference in pseudorapidity. The $\langle\cos(\pi - \Delta\phi)\rangle$ distribution as a quantitative measurement would vary from unity for complete correlation to zero for complete decorrelation. Results from data are compared to an analytical prediction based on BFKL resummation⁷ and the parton showering Monte Carlo HERWIG⁸ in which higher order effects are approximated by a parton shower superimposed on a leading order 2 to 2 parton process.

2 Event Selection and Analysis Cuts

The DØ detector is particularly suited for this measurement owing to its uniform calorimetric coverage to $|\eta| \lesssim 4.0$. The uranium–liquid argon sampling calorimeter facilitates jet identification with its fine transverse segmentation (0.1×0.1 in $\Delta\eta \times \Delta\phi$) and good jet energy and position resolution.

The trigger consists of three levels. The first (L0) requires hits in beam-beam scintillation counters signalling the presence of an inelastic collision. The second level (L1) looks for localized energy deposits in 0.2×0.2 ($\Delta\eta \times \Delta\phi$) towers in the calorimeter. The third level (L2) implements a cone based jet-finding algorithm ($R = 0.7$) using calorimeter cell information. Jets were triggered on out to $|\eta| = 4.0$. We used two triggers specialized for this analysis. One (inclusive) required a single interaction at L0, one trigger tower above 2GeV at L1, and one jet above 12GeV at L2. The other (forward) trigger had the additional pseudorapidity constraints $|\eta| > 2.0$ at L1 and $|\eta| > 1.6$ at L2.

Jet energy scale corrections were applied offline and spurious jets were removed before a minimum E_T cut of 20GeV was applied. Selecting events having at least two jets, we tagged the two jets at the extremes of rapidity and required their boost ($|\bar{\eta}| = \frac{1}{2}|\eta_1 + \eta_2|$) to be less than 0.5 to avoid any trigger bias. Events were removed if either of the tagging jets were located in less well understood detector regions ($1.0 \lesssim |\eta| \lesssim 1.4$). For the forward trigger, one of the two tagging jets was required to be at $|\eta| > 2.25$ to ensure full trigger efficiency, and events from this trigger were used only for $\Delta\eta \geq 4.5$.

3 Results

The azimuthal angular separation, $|1 - \Delta\phi/\pi|$, is plotted for the average of $\Delta\eta$ with unit bins centered at $\Delta\eta = 1$ and 5 in Fig. 1. Since each distribution is normalized to unity, the decorrelation between the two most widely separated jets can be seen in either the relative decline near the peak or the relative increase in width as $\Delta\eta$ increases. Figure 2 shows $\langle \cos(\pi - \Delta\phi) \rangle$ as a function of $\langle \Delta\eta \rangle$. For the data, the error bars represent the statistical and uncorrelated systematic errors added in quadrature. Uncorrelated systematic errors include the effects of the jet position and energy resolution and instrumental backgrounds. Corrections for trigger efficiencies and jet reconstruction efficiency have been also taken into account. Combined corrections are less than 0.01. In addition, the band at the bottom of the plot represents the correlated uncertainties due to the energy scale corrections. Also shown in Fig. 2 are the predictions from the BFKL resummation⁷ and HERWIG⁸ with statistical errors only.

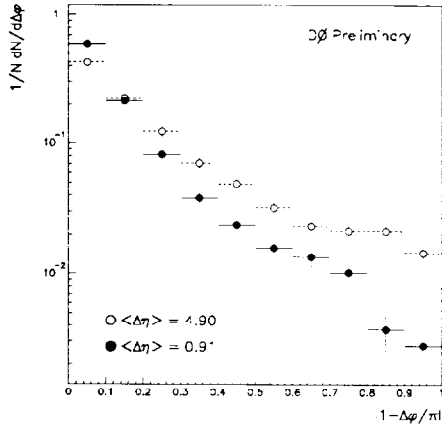


Figure 1: The azimuthal angle difference ($\Delta\phi = \phi_1 - \phi_2$) distribution of the two jets at the extremes of pseudorapidity plotted as $|1 - \Delta\phi/\pi|$ for $\langle\Delta\eta\rangle = 0.91$ ($0.5 < \Delta\eta < 1.5$) and 4.90 ($4.5 < \Delta\eta < 5.5$). The errors are statistical only.

4 Conclusion

We have measured the azimuthal decorrelation of two jets as a function of their rapidity difference using the DØ detector at the Tevatron. The decorrelation increases with increasing $\Delta\eta$. These effects are described well by HERWIG within the uncertainties of the measurement. A theoretical prediction based on BFKL resummation predicts too much decorrelation as the rapidity interval increases.

References

1. A.H. Mueller, H. Navelet, Nucl. Phys. **B282**, 727 (1987).
2. E.A. Kuraev, L.N. Lipatov, V.S. Fadin, Sov. Phys. JETP **45**, 199 (1977); Ya.Ya. Balitsky, L.N. Lipatov, Sov. J. Nucl. Phys. **28**, 822 (1978).
3. W.J. Stirling, Nucl. Phys. **B423**, 56 (1994).
4. V. Del Duca, C.R. Schmidt, Phys. Rev. D **51**, 2150 (1995).
5. DØ Collaboration, S. Abachi *et al.*, Phys. Rev. Lett. **77**, 595 (1996).
6. DØ Collaboration, S. Abachi *et al.*, Nucl. Instrum. Methods A **338**, 185 (1994).
7. V. Del Duca and C.R. Schmidt, private communication.
8. G. Marchesini, B.R. Webber, Nucl. Phys. **B310**, 461 (1988); G. Marchesini *et al.*, Comp. Phys. Comm. **67**, 465 (1992).

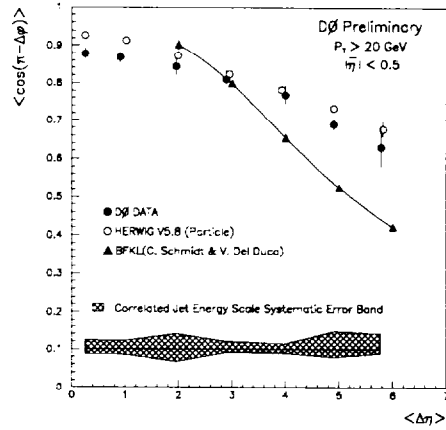


Figure 2: The correlation variable used in this analysis, the average value of $\cos(\pi - \Delta\phi)$ vs. $\Delta\eta$, for the data, HERWIG (particle level), and the BFKL calculations of Del Duca and Schmidt.

COLOR COHERENCE IN $p\bar{p}$ COLLISIONS AT $\sqrt{s} = 1.8$ TeV

DAVID E. CULLEN-VIDAL^b
*Department of Physics, Brown University,
Providence, RI 02912, USA*

We report on two preliminary studies of color coherence effects in $p\bar{p}$ collisions based on data collected by the DØ detector during the 1992–1993 and 1994–1995 runs of the Fermilab Tevatron collider at a center of mass energy $\sqrt{s} = 1.8$ TeV. Demonstration of initial-to-final state color interference effects is done in a higher energy region by measuring spatial correlations between the softer third jet and the second leading- E_T jet in multi-jet events and in a lower energy regime by examining particle distribution patterns in W +Jet events. The data are compared to Monte Carlo simulations with different color coherence implementations and to the predictions of a NLO parton-level calculation.

1 Introduction

Color coherence can be described, in the language of perturbative QCD, as interference among the amplitudes of soft gluons radiated from color-connected partons during the parton cascade process^{1,2}. While quantum mechanical interference effects are expected in QCD, it is of real significance that the experimental results demonstrate that such interference effects survive the hadronization process. An important consequence of color coherence is the *Angular Ordering* (AO) approximation of the sequential parton decays. AO is a leading N_C (number of colors) approximation which requires that opening angles decrease uniformly for successive gluon branchings as the parton cascade evolves away from the hard scattering. AO leads to a suppression of soft gluon radiation in certain regions of phase space.

Evidence has been reported^{3,4,5} for color coherence effects between initial and final states in $p\bar{p}$ interactions by measuring spatial correlations between soft and leading- E_T jets in multi-jet events. In this paper we report updated results from this analysis. A new complementary investigation is also reported here which is sensitive to both perturbative interference effects and the non-perturbative fragmentation process. It takes advantage of the sensitivity of the calorimetry by examining soft particle distributions in W +Jet events and provides additional evidence for color coherence interference between initial and final states. This is the first time color coherence effects are studied using W bosons and jets.

^bRepresenting the DØ Collaboration.

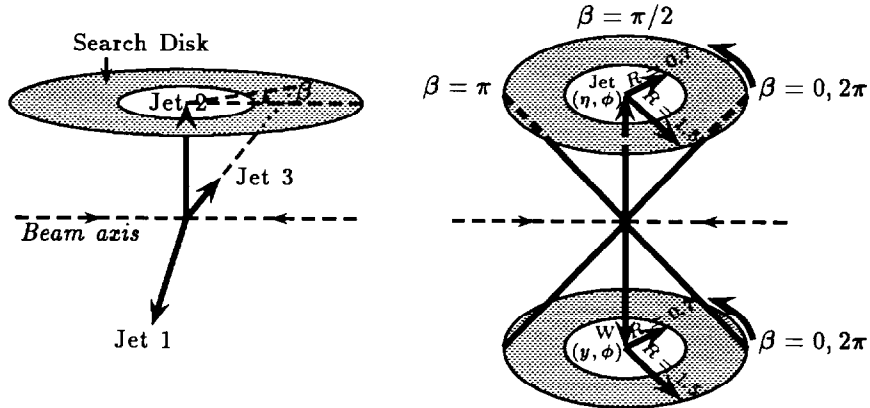


Figure 1: a) Three-jet event topology illustrating the annular search disk (gray area) for studying the angular distribution of the softer third jet around the second leading- E_T jet. b) W +Jet event topology illustrating the annuli and variables for studying the particle flow around the W boson and the leading- E_T jet in the opposite ϕ hemisphere.

2 Method of Analysis

In the multi-jet analysis, events were selected such that the two leading jets had sufficiently high energies so that the coherent radiation formed secondary jets. The events were required to have three or more reconstructed jets which were ordered in E_T and labeled $E_{T1} > E_{T2} > E_{T3}$. The angular distribution, in (η, ϕ) space, of the softer third jet around the second highest- E_T jet was measured using the polar variables $R = \sqrt{(\Delta\eta)^2 + (\Delta\phi)^2}$ and $\beta = \tan^{-1}(\frac{\text{sign}(\eta_2) \cdot \Delta\phi}{\Delta\eta})$; where $\Delta\eta = \eta_3 - \eta_2$ and $\Delta\phi = \phi_3 - \phi_2$, in a search disk of $0.6 < R < \frac{\pi}{2}$ (Fig. 1a). The expectation from color interference is that the rate of soft jet emission around the event plane (i.e., the plane defined by the directions of the second jet and the beam axis: $\beta = 0, \pi, 2\pi$) will be enhanced with respect to that around the transverse plane ($\beta = \frac{\pi}{2}, \frac{3\pi}{2}$).

The data angular distributions are compared to particle-level Monte Carlo simulations (ISAJET⁶, HERWIG⁷ and PYTHIA⁸) that differ in their implementation of color coherence. ISAJET incorporates no color coherence effects, while HERWIG and PYTHIA incorporate interference effects through AO. PYTHIA further allows the choice of not implementing AO and of using either string or independent fragmentation. The data are also compared to the predictions of JETRAD⁹, a parton-level Next-to-Leading Order (NLO) QCD calculation.

In W +Jet events, the pattern of soft particles is measured around both the W boson and the opposing jet in order to observe interference effects. The colorless W boson cannot contribute to color coherence, thereby providing a

template against which the pattern around the jet may be compared. Soft particles in the collider data are approximated in this analysis by projective calorimeter towers of area $\Delta\eta \times \Delta\phi = 0.1 \times 0.1$ with $E_T > 250$ MeV.

Events with the decay $W \rightarrow e + \nu$ are used in this analysis. The W boson is reconstructed from the decay products and the opposing jet is tagged by selecting the highest- E_T jet in the ϕ hemisphere opposite to the W boson. Annular regions similar to those used in the multi-jet study are drawn around both the W boson and the jet in (η, ϕ) space (Fig. 1b).

The angular distributions of calorimeter towers above threshold are measured in these annular regions in a search disk with $0.7 < R < 1.5$. Similar to the multi-jet analysis, we expect the energetic tower distribution around the tagged jet to exhibit a depletion in the transverse plane relative to the event plane (when compared with the W boson distribution) due to initial-to-final state color interference.

The data angular distributions are compared to PYTHIA detector-level Monte Carlo with color coherence effects turned off and on with string and independent fragmentations. To determine the level of residual η -dependent detector effects in the measured patterns, minimum bias events are compared to the W +Jet data. In the minimum bias sample, locations for a fake W boson and jet are placed randomly in each event, weighted to reflect the real W +Jet topology. The same analysis procedure is then applied to these events. Lastly, in order to minimize the statistical uncertainties in the W +Jet sample, the annuli are folded about the ϕ symmetry axis, thereby reducing the β range to $0-\pi$.

3 Event Selection

Multi-jet events were selected using an inclusive jet trigger with E_T threshold of 85 GeV and pseudo-rapidity coverage of $|\eta| < 3.2$. The jets were reconstructed using a fixed-cone clustering algorithm with cone radius $R = 0.5$ (reduced from 0.7 to increase the available phase space for third-jet production.)

After jet energy scale corrections and jet quality cuts were applied, it was required that the transverse energy of the highest- E_T jet of the event be above 115 GeV to avoid any biases introduced by the trigger threshold. The interference effects were studied when the second leading- E_T jet was central ($|\eta_2| < 0.7$) or forward ($0.7 < |\eta_2| < 1.5$). The pseudo-rapidity of the leading jet was not explicitly constrained. The two leading jets were required to be in opposite ϕ hemispheres without imposing any tight back-to-back cut. The third jet was required to have $E_T > 15$ GeV.

For the W +Jet analysis, candidate $W \rightarrow e + \nu$ events were required to

have at least one jet reconstructed using a cone algorithm with $R = 0.7$. Both the electron's E_T and the event's missing E_T (\cancel{E}_T) were required to be greater than 25 GeV.

After electron and jet quality cuts were applied, the rapidity of the W boson was restricted to $|y_W| < 0.5$ and the jet pseudo-rapidity to $|\eta_{Jet}| < 0.5$. The W boson and the jet were only required to be in opposite ϕ hemispheres. Additionally, the z component of the event vertex is restricted to $|z_{vtx}| < 20\text{cm}$ to retain the projective nature of the calorimeter towers.

4 Results

For multi-jet events, the preliminary ratios of the β distributions for the $D\emptyset$ data relative to several Monte Carlo predictions for both central and forward regions are shown in Fig. 2. The HERWIG, ISAJET and PYTHIA simulations have been performed at the particle level, whereas the JETRAD predictions are at the parton level. Detector position and energy resolution effects have been included in all Monte Carlo predictions. The Monte Carlo events were subsequently processed using the same criteria employed for analyzing the data.

The absence of color interference effects in ISAJET results in a disagreement with the $D\emptyset$ data distributions. The data show a clear excess of events compared to ISAJET near the event plane ($\beta = 0, \pi, 2\pi$) and a depletion at the transverse plane ($\beta = \frac{\pi}{2}, \frac{3\pi}{2}$), as expected from initial-to-final state coherent radiation effects. However, HERWIG agrees well with the data. From the DATA/PYTHIA comparisons we see that when we turn off the color coherence effects, PYTHIA disagrees with the data, whereas, it agrees better when the coherence effects are turned on with the other properties of the simulator being the same. Lastly, $\mathcal{O}(a_s^3)$ tree-level QCD describes the coherence effects seen in data reasonably well as shown by the DATA/JETRAD comparisons.

Preliminary ratios of the β distributions for the jet annular region relative to the W boson annulus are shown in Fig. 3a for W +Jet data. When compared to minimum bias data, W +Jet data show a significant enhancement in the event plane while approximately agreeing near the transverse plane, where constructive interference from initial-final state color coherence is at a minimum. In Fig. 3b, PYTHIA with different implementations of AO and fragmentation shows a decrease in the event plane relative to the transverse plane as AO is turned off and independent fragmentation is implemented. In Fig. 3c, PYTHIA with AO and string fragmentation is in qualitative agreement with the W +Jet data, exhibiting a similarly shaped curve.

DO PRELIMINARY

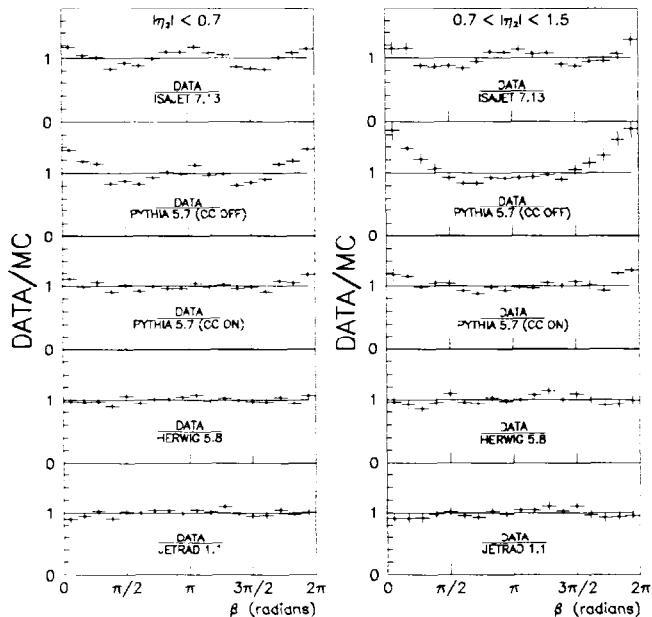


Figure 2: Ratio of β distributions between multi-jet data and Monte Carlo predictions for both central and forward pseudo-rapidity regions. All errors are statistical.

5 Conclusions

Color coherence effects in $p\bar{p}$ interactions have been observed and studied in two analyses by the DØ collaboration. Using multi-jet events we have measured the spatial correlations between the second and the third leading- E_T jets and have compared the data distributions to several MC predictions with different implementations of color coherence. Monte Carlo simulations that implement color interference effects (via AO) reproduce the data angular distributions reasonably well, with HERWIG best representing the data. Furthermore, preliminary results indicate that coherence effects as predicted by a NLO calculation are also in agreement with the data.

We have also presented the first preliminary results on color coherence effects in W +Jet events. Data show an enhancement of soft particle radiation in the event plane with respect to the transverse plane which is qualitatively consistent with PYTHIA predictions using the AO approximation and string fragmentation.

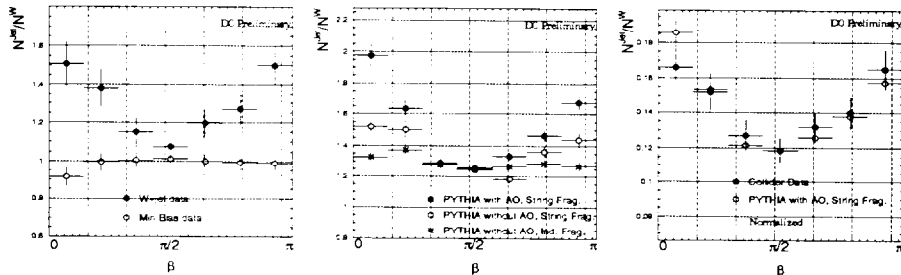


Figure 3: a) Ratios of data folded β distributions (Jet/W) in W +Jet (filled circles) and minimum bias (open circles) collider data. b) Detector-level PYTHIA with AO on and string fragmentation (filled circles), AO off and string fragmentation (open circles) and AO off and independent fragmentation (asterisks). c) Comparison of data (filled circles) and PYTHIA with AO on and string fragmentation. All errors are statistical.

Acknowledgments

We acknowledge the support of the US Department of Energy and the collaborating institutions and their funding agencies in this work.

References

1. Ya.I. Azimov, Yu.L. Dokshitzer, V.A. Khoze, and S.I. Troyan, *Phys. Lett.* **B165**, 147 (1985); *Sov. Journ. Nucl. Phys.* **43**, 95 (1986).
2. R.K. Ellis, G. Marchesini, and B.R. Webber, *Nucl. Phys.* **B286**, 643 (1987).
3. F. Borchering (DØ Collaboration), *Proceedings of the 9th Topical Workshop on Proton-Antiproton Collider Physics*, Tsukuba, Japan, 218, 18–22 Oct. 1993.
4. F. Abe *et al.* (CDF Collaboration), *Phys. Rev.* **D50**, 5562 (1994).
5. S. Abachi *et al.* (DØ Collaboration), *Fermilab-Conf-95/182-E*; *Fermilab-Conf-96/278-E*.
6. F.E. Paige and S.D. Protopopescu, BNL report No. 38034 (1986).
7. G. Marchesini and B.R. Webber, *Nucl. Phys.* **B310**, 461 (1988).
8. H.-U. Bengtsson and T. Sjöstrand, *Computer Physics Commun.* **46** (1987) 43
9. W.T. Giele, E.W.N. Glover, and D.A. Kosower, *Phys. Rev.* **D46**, 1980 (1992); *Nucl. Phys.* **B403**, 633 (1993); *Phys. Rev. Lett.* **73**, 2019 (1994).

RAPIDITY GAPS IN HARD PROCESSES AT DØ

JILL PERKINS

University of Texas at Arlington, P.O. Box 19059, Arlington, Texas 76019

for the DØ Collaboration

Latest results on jet production with rapidity gaps at the Fermilab Tevatron Collider are presented. Jet production via color-singlet exchange at high momenta transfer is observed as a class of events with low particle multiplicity (or rapidity gaps) between the two highest transverse energy jets. The particle multiplicity in various regions, and the dependencies on jet pseudorapidity separation and jet transverse energy are studied for these events. Results from two classes of dijet events with one or two forward rapidity gaps are also presented. The topology of these events is consistent with expectations for hard single diffraction and hard double pomeron exchange processes, respectively.

1 Rapidity Gaps Between Jets

Two jets separated by a rapidity gap, defined as a region of rapidity (or pseudorapidity η) containing no final-state particles, has been proposed as a signature for jet production via the exchange of a color-singlet (colorless) object^{1,2}. Recent experiments provide evidence for a strongly-interacting color-singlet^{3,4,5,6}. We present new results on color-singlet exchange from the 1994-95 collider run.

Comparing particle multiplicities is a convenient method for distinguishing color-singlet exchange from the color-octet background. Particle multiplicity between the two leading transverse energy (E_T) jets is approximated by counting electromagnetic (EM) calorimeter towers (0.1×0.1 in $\eta - \phi$) with $E_T > 200$ MeV (n_{cal}) and central tracks (n_{trk}). We present a new measurement of color-singlet exchange as a function of the E_T of the two leading jets. The fractional excess above a parametrization of the background multiplicity is observed to be roughly constant and on the order of 1% of the inclusive dijet sample over a significant range of E_T , consistent with a strongly-interacting color-singlet exchange process. Future studies will include an η dependence measurement.

Color exchange fluctuations can also produce rapidity gaps. Therefore, the presence of a rapidity gap is not sufficient to tag an event as color-singlet exchange. It is interesting to study the characteristics of a rapidity gap sample (with $n_{cal} = n_{trk} = 0$ between the jets) as compared to a background sample (with $n_{cal} = 3$ and $n_{trk} > 2$ between the jets). We can also include a 'quiet' sample (with $n_{cal} = 0$ and $n_{trk} > 0$, or $n_{cal} = 1$ and $n_{trk} = 0$) to study our efficiency for tagging color-singlet events. For this comparison, n_{cal} is

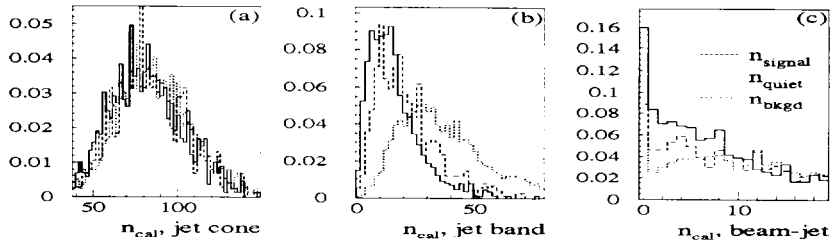


Figure 1: Multiplicity (n_{cat}) a) in cone of leading jets, b) in band of jets excluding the jets, c) in beam-jet region

the number of EM calorimeter towers with energy (E) $>$ 200 MeV . Using an energy threshold provides greater sensitivity for tagging forward particles. The rapidity gap sample is estimated to be about 90% color-singlet exchange, while the background sample is estimated to be about 90% color exchange. The multiplicity (n_{cat}) in different $\eta - \phi$ regions is compared for the rapidity gap sample, the background sample, and the quiet sample. Figures 1(a)-(c) show the multiplicity in: a) the cone ($R = \sqrt{\Delta\eta^2 + \Delta\phi^2} = 0.7$) of the two leading jets, b) the η band ($\eta_{jet} \pm 0.7$) of the jets, excluding the jet cone, and c) the beam-jet region ($|\eta| > |\eta_{jet}| + 0.7$).

These distributions show that the multiplicity in an event is correlated across $\eta - \phi$. Rapidity gap events tend to have lower multiplicities than non-gap events in most event regions. These correlations are presumably due to differences between color and color-singlet exchange processes. In the future, the internal jet structure and more detailed multiplicity correlations will be studied.

2 Forward Rapidity Gaps

Hard diffraction has recently been defined as events which contain a hard scattering opposite a large rapidity gap. Jet production in diffractive events has been observed by both UA8⁷ and HERA⁸. CDF has set an upper limit of 0.75% of dijet events due to hard single diffraction⁸. Observations and measurements of hard diffraction give new insight into the pomeron.

The DØ collaboration implemented several triggers to search for hard single diffraction and hard double pomeron exchange in the 1994-96 running period. The triggers utilized the Level 0 detectors, which are arrays of scintillating tiles surrounding the beam pipe on either side of the central calorimeter,

and are used for tagging inelastic scattering. An inclusive trigger ignored Level \emptyset . A single veto trigger vetoed events with hits in one array. A double veto trigger vetoed events with hits in both arrays. Figure 2 shows a two dimensional multiplicity distribution for the inclusive trigger for EM calorimeter towers with $E > 200$ MeV ($n_{cal(EM)}$) and hadronic calorimeter towers with $E > 600$ MeV ($n_{cal(HAD)}$) in the region $2 < |\eta| < 4$ for the minimum multiplicity hemisphere of the detector. The spike at zero multiplicity shows there is an excess of events with a forward rapidity gap in both the electromagnetic and hadronic calorimeters. Other studies show that these rapidity gap events are also quiet in other detectors such as the forward tracking and forward muon system. The fractional excess observed in the forward region is $0.67 \pm 0.05\%$, where the error includes only statistical uncertainties and a systematic uncertainty based on the choice of range for the fit.

The fraction of single gap events in the inclusive sample can be measured, and then combined with the measured fraction of double gap events in the single veto sample to give a fraction of double gap events in the inclusive sample. The double gap events are present at a rate of $O(10^{-6})$ of the inclusive sample. Further study is required to associate this rate with hard double pomeron exchange.

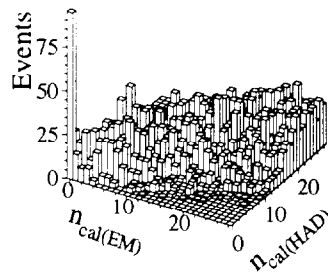


Figure 2: Multiplicity Distribution in Inclusive Sample

References

1. Yu.L. Dokshitzer, V.A. Khoze and S.I. Troian, *Proceedings of the 6th International Conference on Physics in Collisions* (1986), ed. M. Derrick (World Scientific, 1987).
2. J.D. Bjorken, *Phys. Rev. D* **47**, 101 (1992).
3. S. Abachi *et al.* (DØ Collaboration), *Phys. Rev. Lett.* **76**, 734 (1996).
4. M. Derrick *et al.* (ZEUS Collaboration), *Phys. Lett. B* **369**, 55 (1996).
5. F. Abe *et al.* (CDF Collaboration), *Phys. Rev. Lett.* **74**, 855 (1995).
6. S. Abachi *et al.* (DØ Collaboration), *Phys. Rev. Lett.* **72**, 2332 (1994).
7. A. Brandt *et al.* (UA8 Collaboration), *Phys. Lett. B* **297**, 417 (1992).
8. K. Goulianos, *Proceedings of the 10th Topical Workshop on Proton-Antiproton Collider Physics* (1995), ed. R. Raja, J. Yoh, (AIP Press, 1996).